Hydrogels containing metallic glass sub-micron wires for regulating skeletal muscle cell behavior

Journal:	*Biomaterials Science*
Manuscript ID:	BM-ART-06-2015-000215.R1
Article Type:	Paper
Date Submitted by the Author:	03-Aug-2015

Complete List of Authors:	Ahadian, Samad; Tohoku University, WPI-AIMR Banan Sadeghian, Ramin; Tohoku University, WPI-AIMR Yaginuma, Shin; Tohoku University, WPI-AIMR Ramón-Azcón, Javier; Tohoku University, WPI-AIMR Nashimoto, Yuji; Tohoku University, Graduate School of Environmental Studies Liang, Xiaobin; Tohoku University, WPI-AIMR Bae, Hojae; Konkuk University, College of Animal Bioscience and Technology, Department of Bioindustrial Technologies Nakajima, Ken; Tohoku University, WPI-AIMR Shiku, Hitoshi; Tohoku University, Graduate School of Environmental Studies Matsue, Tomokazu; Tohoku University, WPI-AIMR; Tohoku University, Graduate School of Environmental Studies Nakayama, Koji; Tohoku University, WPI-AIMR Khademhosseini, Ali; Harvard Medical School,

Biomaterials Science

ARTICLE

Hydrogels containing metallic glass sub-micron wires for regulating skeletal muscle cell behavior

Received 00th January 20xx,
Accepted 00th January 20xx

DOI: 10.1039/x0xx00000x

www.rsc.org/

Samad Ahadian,[a,†] Ramin Banan Sadeghian,[a,†] Shin Yaginuma,[a] Javier Ramón-Azcón, [a] Yuji Nashimoto,[b] Xiaobin Liang,[a] Hojae Bae,[c] Ken Nakajima,[a] Hitoshi Shiku,[b] Tomokazu Matsue,[a,b] Koji S. Nakayama[a] and Ali Khademhosseini[*a,c,d]

Hydrogels with tunable electrical and mechanical properties have a wide range of biological applications in tissue engineering, biosensing, and biorobotics. In this work, palladium-based metallic glass sub-micron wires (PdMGSMWs) were employed to enhance the conductivity and mechanical strength of gelatin methacryloyl (GelMA) gels. The values of electrical resistivity and stiffness of hybrid GelMA-PdMGSMWhydrogels were varied by the concentration of the sub-micron wires in the gels. Compared with pristine GelMA gels, hybrid GelMA-PdMGSMWgels were more efficient in regulating adhesion and spreading of C2C12 myoblasts. Formation, contractility, and metabolic activity of C2C12 myotubes in GelMA hydrogels also increased upon inclusion of the PdMGSMWs and applying electrical stimulation. The latter phenomenon is likely because of the electrical conductivity of hybrid GelMA gels.

Keywords: Cell encapsulation, Electrical stimulation, Hydrogel, Metallic glass, Muscle, Scaffold.

Introduction

Hydrogels have been extensively used as scaffolds in regenerative medicine applications due to their high hydration, biocompatibility, and biodegradability [1-3]. However, they often need to be electrically conductive and mechanically robust to be capable of regulating behaviors of electrically active cells, for example neural and skeletal muscle cells [4]. In particular, conductive hydrogels are helpful in tissue fabrication because they allow enhanced electrical stimulation (ES) of cells [5-7]. Conductive and mechanically robust gels have other applications in biomedicine, for instance in biosensing [8, 9], as functional materials in electronics-biology interfaces [10, 11], as bioactuators [12, 13], and in drug delivery [14, 15].

Nanomaterials have been employed to increase the mechanical characteristics and conductivity of scaffolds [12]. For instance, we recently showed that carbon nanotubes (CNTs) can be incorporated into gelatin methacryloyl (GelMA) making it an electrically conductive hydrogel with moderately high Young's modulus for cell encapsulation studies [16]. The CNT network structure in GelMA reinforced the gel-CNT materials. Following this work, we anisotropically aligned CNTs in GelMA hydrogels. GelMA-aligned CNT hydrogels resulted in anisotropically conductive hydrogels compared with pure GelMA and GelMA gels having random CNTs [17]. GelMA gels containing aligned CNTs were more efficient in the fabrication of muscle tissues using the ES applied along the aligned CNTs compared with pristine and GelMA-random CNT hydrogels, most likely because of the superior and anisotropic electrical conductivity of GelMA-aligned CNT hydrogels. Gold nanomaterials have also been employed to enhance the electrical conductivity of alginate hydrogels [18]. Hybrid alginate-gold hydrogels were superior to pristine alginate hydrogels in ES of heart and neural cells. Other commonly used nanomaterials to enhance the properties of hydrogels include carbon nanofibers [19], graphene-based nanomaterials [20], and polymeric nanosheets [21].

Metallic glasses are amorphous alloys having a glass transition temperature. They possess unique properties, such as ultrahigh strength and flexibility compared with conventional crystalline metals [22]. Other advantages of metallic glasses over conventional metals are high wear and corrosion resistance. This is because they lack crystal dislocations and grain boundaries, which often lead to a decreased strength and corrosion resistance of materials [23]. They have particularly high corrosion resistance in biological media compared with conventional crystalline metallic biomaterials [24, 25]. In addition, they can be formed with a wide range of alloy compositions allowing the design and fabrication

[a] *WPI-Advanced Institute for Materials Research, Tohoku University, Sendai 980-8577, Japan.*
[b] *Graduate School of Environmental Studies, Tohoku University, Sendai 980-8579, Japan.*
[c] *College of Animal Bioscience and Technology, Department of Bioindustrial Technologies, Konkuk University, Hwayang-dong, Kwangjin-gu, Seoul 143-701, Republic of Korea.*
[d] *Biomaterials Innovation Research Center, Division of Biomedical Engineering, Department of Medicine, Brigham and Women's Hospital, Harvard Medical School, Boston, MA 02139, USA; Harvard-Massachusetts Institute of Technology Division of Health Sciences and Technology, Massachusetts Institute of Technology, Cambridge, MA 02139, USA; Wyss Institute for Biologically Inspired Engineering, Harvard University, Boston, MA 02115, USA; Department of Physics, Faculty of Science, King Abdulaziz University, Jeddah 21569, Saudi Arabia.*
† These authors contributed equally to this work.
Electronic Supplementary Information (ESI) available: [details of any supplementary information available should be included here]. See DOI: 10.1039/x0xx00000x

of these materials with non-toxic elements. In our previous works, we fabricated metallic glass sub-micron wires (MGSMWs) having extremely long length and structural stability [26-28]. However, to our knowledge, there has been no report on the biomedical applications of MGSMWs. We believe that hybrid MGSMW-hydrogel scaffolds can provide electrically conductive and mechanically strong gels for different biomedical applications. Compared with other aforementioned nanomaterials, MGSMWs are easier to fabricate and cheaper. Furthermore, large quantities of MGSMWs can be obtained in a short time without using toxic chemicals, making them suitable for biomedical applications without the need of further purification. MGSMWs can be provided with tunable composition and physical characteristics (e.g. diameter and length) making them promising nanomaterials for various biomedical applications. Interestingly, alloys of Pd are sensitive to hydrogen in molecular form. Upon adsorption of hydrogen, the Pd lattice expands resulting in an increase in the electrical resistance of the alloy that is proportional to the amount of dissolved hydrogen in the medium [29]. Therefore, monitoring the resistance of PdMGSMWs can be a useful technique to quantify the biodegradation of certain type of implants, such as magnesium that release hydrogen upon the degradation.

In this investigation, we used PdMGSMWs to enhance the conductivity and stiffness of GelMA gels. Electrical properties and stiffness of GelMA gels containing PdMGSMWs and pure GelMA hydrogels were measured and compared. Biocompatibility and the ability of hybrid GelMA-PdMGSMW gels to regulate the behaviors of skeletal muscle cells were also demonstrated.

Materials and methods

Materials

Materials and their suppliers are listed as follows: Indium tin oxide (ITO)-coated glass slides (Sanyo Vacuum Industries Co., Ltd., Japan); penicillin/streptomycin (P/S); methacrylic anhydride; and gelatin (Sigma-Aldrich Chemical Co., USA); fetal bovine serum (FBS) (Bioserum, Japan); 2-hydroxy-1-[4-(2-hydroxyethoxy)phenyl]-2-methyl-1-propanone (Irgacure 2959) (Ciba Chemicals, Osaka, Japan); and trypsin/EDTA; Dulbecco's modified Eagle medium (DMEM); MEM nonessential amino acid; insulin; MEM essential amino acid (Invitrogen, USA).

Synthesis of GelMA hydrogel

GelMA prepolymer was synthesized as previously described [30]. Briefly, gelatin (6 g) was mixed with methacrylic anhydride (12 mL) in Dulbecco's phosphate-buffered saline (DPBS) for 1 hr at 50°C to obtain ~80% degree of amine conversion. A 12-14 kDa dialysis membrane was used to dialyze the mixture against distilled water (at 40°C) for 1 week. The mixture was then lyophilized for 1 week. GelMA polymer and 1% (w/v) photoinitiator (Irgacure 2959) were dissolved in DPBS at 60°C.

Synthesis and characterization of PdMGSMWs

A master alloy of $Pd_{42.5}Cu_{30}Ni_{7.5}P_{20}$ (atomic %) was supplied by the group of Professor Osami Haruyama, Tokyo University of Science, Japan [31]. PdMGSMWs were created by gas atomization of the $Pd_{42.5}Cu_{30}Ni_{7.5}P_{20}$ alloy [27]. About 3 g of the alloy was melted in a quartz crucible using an induction heating system. The melted alloy was forced through the crucible nozzles and was blown into particles and wires by high speed gas jets. Size and shape of the wires mainly depend on the viscosity of melted alloys and the pressure of gas jets. Here, the heating temperature and gas pressure were 793 K and 10 MPa, respectively, to fabricate the PdMGSMWs.

Electrical characterizations of GelMA and GelMA-PdMGSMW gels

A parallel plate capacitor was fabricated using ITO glass slides to perform I-V characterization as well as electrochemical impedance spectroscopy on GelMA and GelMA containing PdMGSMWs. Hydrogel samples to be characterized were sandwiched between two ITO electrodes. No cells were incorporated in the hydrogels during the electrical characterization. The interelectrode spacing and electrode effective area were 50 µm and 1.2 mm^2, respectively. Direct current (DC) characterization was performed using a single source-measure unit of a semiconductor parameter analyzer (Model 4200-SCS Parameter Analyzer, Keithley Inc., USA). I-V curves were recorded upon the application of a double voltage sweep from -6.0 V to +6.0 V. The voltage sweep amplitude and time step were 0.1 V and 100 ms, chosen small enough and large enough, respectively, to reduce the unwanted capacitive charge and discharge currents. Frequency-domain measurements were taken using a single source-measure unit of an LCR meter (Model 4263B, Agilent Technologies, Japan) at different frequencies and a test signal level of 1 V_{rms}.

Mechanical characteristics of GelMA and GelMA-PdMGSMW gels

The force-deformation curves obtained using atomic force microscopy (AFM) (MultiMode 8 AFM (Bruker Co., USA)) were used to quantify the mechanical characteristics of GelMA and GelMA-PdMGSMW gels [32]. A 1.0-µm radius colloidal probe (PT.GS, Novascan Technologies, USA) was used in the AFM cantilever. The thermal noise method was used to obtain the spring constant of cantilever [33]. The Derjaguin, Muller, and Toporov theory [34] was employed to calculate the Young's modulus values.

Cell culture

C2C12 myoblasts and NIH 3T3 fibroblasts were cultured in DMEM contained 1% P/S and 10% FBS. Trypsinization was done using trypsin/EDTA after the cells reached ~80% confluency. All cell culture experiments were performed in accordance with the guidelines set by Tohoku University in an approved biosafety level 2 laboratory.

Preparation of cell-laden hydrogels

For the cell encapsulation in pristine GelMA and GelMA-PdMGSMW gels, the cells (cell density=1 × 10^7 cells/mL) were

suspended in 5% (w/v) prepolymers and then thoroughly mixed with the gels to make a homogeneous cell-laden prepolymer. The samples were then subjected to the UV light (Hayashi UL-410UV-1; Hayashi Electronic Shenzen Co., Japan) for 60 s to make the three-dimensional (3D) cell-laden hydrogels. The UV exposure time was optimized to be sufficient to crosslink the gels while do not affect the viability of cells within the gels. The preparation method of 3D cell-laden GelMA-PdMGSMW hydrogels along with the phase contrast images of 3D cell-laden GelMA-PdMGSMW hydrogels at days 0 and 1 are shown in Supplementary data, Figures S1 and S2.

Analysis of cell viability and proliferation

Live cells in 3D pristine GelMA or hybrid GelMA-PdMGSMW hydrogels were identified using a calcein AM/ethidium homodimer live/dead assay (Invitrogen, USA). Five 10x magnified pictures of two replicated experiments were used for the quantification of live cells using NIH ImageJ software. The cell proliferation rate on each day of culture was calculated as the ratio of the number of live cells on that day to the number of live cells on day one of culture.

Immunostaining of C2C12 myoblasts

C2C12 myoblasts were stained as previously described [35, 36]. Briefly, the cells were treated using 3-4% paraformaldehyde for 12 min. The cells were permeabilized using 0.3% Triton X-100 in 5 min. The samples were then treated with 5% bovine serum albumin in DPBS for 15 min to block unspecific binding of the antibodies. The immunostaining procedure was done with AlexaFluor® 594 (Invitrogen, USA) and 4,6-diamidino-2-phenylindole (DAPI) (Vector Laboratories Inc., USA) to quantify F-actin and cell nucleus, respectively. The aspect ratio parameter is defined as the ratio of long axis to short axis of the cell nucleus. Two hundred cells from two independent experiments were considered to determine the aspect ratio values. The aspect ratio of C2C12 myoblasts was calculated with NIH ImageJ software.

Immunostaining of C2C12 myotubes

C2C12 myotubes were fixed, permeabilized, and blocked as detailed in the previous section. Fast skeletal myosin of myotubes was revealed using a mouse antibody (ab-7784, Abcam®) diluted 1000 times in DPBS at 4°C for 24 hr. After 3 times washing the sample with DPBS, it was exposed to the goat anti-mouse AlexaFluor® 488 antibody (Invitrogen, USA) diluted 1000 times in DPBS at 37°C for 1 hr. DAPI and Alexa Fluor® 594 were used to show nuclei and F-actin of C2C12 myotubes, respectively.

Electrical stimulation of C2C12 myotubes

C2C12 myotubes were electrically stimulated using two Pt electrode bands (10 mm apart) deposited on a glass slide using conventional lithography technique [37]. During the ES of C2C12 myotubes, differentiation medium (DMEM with 1 nM insulin, 1% MEM with nonessential amino acid, 2% MEM essential amino acid, 2% horse serum, and 1% P/S) was used. A function generator (WF 1946B Multifunction Synthesizer; NF Co., Japan) was used to apply electrical pulses. A specified ES regime (voltage 4 V, frequency 1 Hz, and duration 10 ms for 2 continuous days) was applied at day 8 of culture. This ES regime was in the range of physiologically relevant stimulations (i.e. frequency 0.5-5 Hz, pulse amplitude, and duration) that activate an action potential in skeletal muscle cells releasing calcium ions from the sarcoplasmatic reticulum and subsequently cause muscle contraction [38]. Stimulus polarity was changed every 8 hr over the stimulation time.

RNA extraction and complementary DNA (cDNA) synthesis

Liquid nitrogen was used to fix the cells. The cells were then powdered using a pestle and mortar. β-mercaptoethanol was used to extract the RNA from the cells. The RNA was then purified using an RNeasy© Micro Kit (Qiagen, Netherlands). A QuantiTect Reverse Transcription kit (Qiagen, Netherlands) was used to reverse-transcribe 3 μg of total RNA. 12 μL of sample was diluted with gDNA wipeout buffer (4 μL) and RNase-free water (14 μL) to synthesize the cDNA. The sample was kept at 42°C for 2 min and then the temperature was decreased to 4°C. The Reverse Transcriptase primer mix and Quantiscript Reverse Transcriptase were mixed with the sample and it was kept at 42°C for 15 min and then heated up and kept at 95°C for 3 min. The sample was incubated at 4°C.

PCR experiment

The primers (Operon Biotechnologies, Japan) had the sequences detailed in Table 2 [6, 39]. The PCR was done by the LightCycler FastStart DNA Master SYBR Green 1 reaction mix (Roche, Germany) (14 μL), Roche LightCycler 1.5 (Roche, Germany) cDNA (2 μL), and primer set (2 μL). A denaturation procedure was performed at 95°C for 10 min. The PCR was then done over 45 cycles using a melting curve (95°C for 10 s, 62°C for 10 s, and 72°C for 20 s). The gene expression level was normalized to that of the GAPDH gene [40]. The PCR experiments were repeated four times.

Oxygen flux measurements

The fabrication of Pt microelectrodes for the scanning electrochemical microscopy (SECM) measurements was described elsewhere [41]. The Pt electrodes with tip radius of 20 μm as measured by the cyclic voltammetry in a 4.0 mM $K_4Fe(CN)_6.3H_2O$, 0.1 M KCl solution were used for the SECM measurements. The SECM measurements were done in a DPBS solution containing 11.2 mM D-Glucose, 100 mM KCl, 25 mM $Na_2HPO_4.12H_2O$ and 25 mM NaH_2PO_4 in a closed chamber at ambient temperature. The samples were kept 60 min in this medium prior to the experiments to stabilize them [42]. The reference electrode was Ag/AgCl electrode, while the Pt microelectrode was the working electrode. The oxygen reduction currents were measured at -0.50 V versus Ag/AgCl using a picoammeter (428MS, Keithley Inc., USA). The Pt microelectrode vertically scanned the samples until the

distance 500 µm from the sample surface at a constant scan rate 10 µm s^{-1}. The oxygen flux values were calculated by the Fick's law as follows:

$$f_s = D \times \Delta C/\Delta z = D \times \Delta I/\Delta z \times C^*/I^*,$$

where f_s is the oxygen flux (mol cm^{-2} s^{-1}), D is the oxygen diffusion coefficient (2.1×10^{-5} cm^2 s^{-1}), C* is the bulk oxygen concentration, I* is the current response of bulk oxygen, and $\Delta I/\Delta z$ is the slope of current versus distance plot. This model has been widely used in SECM experiments to calculate mass transfer rate of chemicals [42]. The reported oxygen flux values were the average of 6 independent measurements in forward and backward scanning modes relative to the sample position.

Statistical analysis

Statistically significant differences were revealed using a one-way ANOVA and a post hoc analysis. A Tukey-Kramer all pairs post hoc analysis was used for the groups having equal variances and normal distribution, otherwise we used a Steel-Dwars all pairs non-parametric post hoc analysis. All repeated data sets are shown as the average ± standard deviation and $p<0.05$ were labeled as significant.

Results and discussion

Here, PdMGSMWs were produced from the gas atomization of $Pd_{42.5}Cu_{30}Ni_{7.5}P_{20}$ (atomic %) alloy. This is a facile and versatile technique to produce high quantities of wires of different metallic glasses [27]. Scanning electron microscopy (SEM) pictures of the sub-micron wires (Figure 1a) revealed that they were highly dense and had a smooth surface. The distribution of PdMGSMW diameters is nearly gaussian, as shown in Figure 1b. In addition, we could easily handle the PdMGSMWs using tweezers.

GelMA and GelMA-PdMGSMW gels containing 0.5 and 1.0 mg/mL PdMGSMWs were prepared to evaluate the effect of PdMGSMWs on the electrical properties of GelMA hydrogel. The hydrogels were confined between two glass slides coated with ITO to obtain accurate conductivity measurements for hydrogels. The electrode area and spacing of the devices were 1.2 cm^2 and 50 µm, respectively. Figure 1c summarizes the results of electrical measurements. As shown in Figure 1c-1, the current-voltage (I-V) curve of the device containing pristine GelMA exhibited a nonlinear behavior. As the applied voltage exceeded 3 V, GelMA became conductive due to electrolysis of the medium (*i.e.* DPBS). Before the occurrence of electrolysis, pristine GelMA had a high resistance that could not be quantified with our measurement system. In contrast, the hybrid GelMA-PdMGSMW hydrogels displayed an ohmic behavior with an increased conductivity. The resistances of hybrid GelMA-PdMGSMW hydrogels were extracted from the slope of the plots and almost inversely proportional to the amount of embedded wires. The ohmic resistances were 19.2 and 33.5 Ω for 1.0 and 0.5 mg/mL of PdMGSMWs in hybrid gels, respectively. The observed discrepancy in the above trend was mainly contributed to the inhomogeneity of PdMGSMW spreading in GelMA hydrogels. Table 1 shows the resistivities of the hybrid hydrogels versus the concentration of embedded PdMGSMWs measured at 100 Hz. Taken together, these results demonstrate the feasibility of tuning the conductivity of GelMA hydrogels by the concentration of embedded nanowires.

The Bode plots of the device impedance (Figure 1c-2) demonstrate that pristine GelMA gels showed a purely resistive behavior at frequencies above 5 kHz. In other words, the magnitude of impedance, |Z|, remained constant while its phase, ∠Z, became zero. In comparison, the GelMA-PdMGSMW showed less resistance throughout the studied range of frequency.

We applied the measured frequency response to a Randels' equivalent circuit and computed the variation of parallel resistance, R_p, and capacitance, C_p, with frequency (Figure 1c-3) similar to a previous study [43]. The series resistance, R_s, for all underlying gels was less than an ohm and therefore negligible. The R_p values at all measured frequencies for hybrid gels were significantly lower than those for pristine GelMA gels. Note that the mobility of ions in the hydrogels are limited, as a result, not all of the electrode area was charged by ions at high frequencies causing the capacitance to roll-off in a similar fashion to electrolytic capacitors. These results clearly show the significant role of PdMGSMWs to enhance the electrical conductivity of GelMA hydrogels.

An AFM-based technique was employed to reveal the stiffness of pristine GelMA and GelMA-PdMGSMW hydrogels containing 0.1 and 0.2 mg/mL PdMGSMWs. The stiffness for pure GelMA was 0.47±0.12 kPa, while it was increased to 1.03±0.64 and 3.99±1.35 kPa for GelMA-PdMGSMW hydrogels reinforced with 0.1 and 0.2 mg/mL PdMGSMWs, respectively (Supplementary data, Figure S3 and Figure 1d), likely due to the web-like structure of PdMGSMWs within hydrogels. The pristine GelMA was too soft requiring a specific AFM cantilever for characterizing its mechanical properties. The cantilever was not able to quantify mechanical properties of hybrid GelMA gels containing more than 0.2 mg/mL PdMGSMWs. Therefore, mechanical properties of hybrid gels were reported up to 0.2 mg/mL PdMGSMW concentration. A common approach to increase the mechanical properties of hydrogels is to use higher concentration or molecular weight of hydrogel precursors, which often limits their applications for cell-based studies. For instance, increasing the stiffness of GelMA gels by adding the concentration or molecular weight of functional groups decreased cell migration, viability, and proliferation in the hydrogels [44]. In this regard, PdMGSMWs show a significant effect on mechanical properties of hydrogels. In addition, we did not observe any structural change in GelMA-PdMGSMW hydrogels over their culture time because of stable and interconnected network of the wires in the gels.

One mg/mL PdMGSMWs were sufficient to increase electrical conductivity and stiffness of GelMA hydrogel significantly. Therefore, we assumed that this PdMGSMW concentration was selected for following cell-based studies assuming that it would have significant effects on cellular behaviors cultured in the gel. To ensure that the developed gels could be used for cell-based applications, we evaluated

the biocompatibility of hybrid GelMA-PdMGSMW hydrogels (Figure 2). The 3D cell-laden hydrogels were prepared as shown in Supplementary data, Figure S1. The differences between the viability of fibroblasts in pristine GelMA and GelMA-1.0 mg/mL PdMGSMW hydrogels were not significant during 2 days of culture (Figure 2c). Even though the PdMGSMW concentrations of less than 1.0 mg/mL had significant effects on the electrical and mechanical properties of hybrid GelMA-PdMGSMWgels, we chose the highest concentration of PdMGSMWs used in hybrid GelMA-PdMGSMW gels (*i.e.* 1.0 mg/mL) as it maintained a high level of biocompatibility. A high percentage of viable cells encapsulated in GelMA-1.0 mg/mL PdMGSMW gels at days 1 and 2 of culture (96.7±2.6 and 97.1±0.9%, respectively) indicated that PdMGSMWs are not cytotoxic. The biocompatibility of metallic glasses to cells and tissues has been shown both *in vitro* and *in vivo* conditions [45, 46]. Interestingly, metallic glasses can be biodegradable and their biodegradation rate can be tuned with minimal hydrogen release, which is difficult to obtain using crystalline alloys [47, 48]. Results of muscle cell proliferation (Figure 2d) showed that there was no significant difference between the cell proliferation in the pristine GelMA and GelMA-PdMGSMW hydrogels.

We further evaluated the effect of adding PdMGSMWs to hydrogels as a tool to regulate the behavior of C2C12 myoblasts. The morphology, adhesion, and spreading of C2C12 myoblasts within pristine GelMA and GelMA-PdMGSMW hydrogels were assessed at days 1 and 2 of culture by visualizing the cytoskeletal structures of cells (Figure 2b). The C2C12 myoblasts cultured in GelMA-PdMGSMW hydrogels were more elongated than those cultured in pristine GelMA hydrogels. The aspect ratio values of cell nuclei were 1.36±0.26 and 1.32±0.15 for muscle cells encapsulated in pristine GelMA hydrogels at days 1 and 2 of culture, respectively, while these values were 2.88±0.88 and 2.95±0.71 for muscle cells cultured in GelMA-PdMGSMW hydrogels (Figure 2e). This is likely due to combined morphological and electrical characteristics of PdMGSMWs in GelMA hydrogels for muscle cells as to increase favorable sites for the cellular adhesion and elongation. We also previously confirmed that C2C12 myoblasts are highly sensitive to morphology and conductivity of substrates and showed higher adhesion and spreading on the conductive surfaces with CNTs compared to the surfaces without CNTs [21]. It has been demonstrated that elongation of C2C12 myoblasts is one of the earliest stages of myotube formation [49, 50]. Cell nuclear shape has been shown to be correlated with cell adhesion, spreading, and differentiation [30]. Pictures of C2C12 myoblasts at day 0 of differentiation are shown in Figure S4. The C2C12 myoblasts in both pristine GelMA and GelMA-PdMGSMW hydrogels were reached almost a complete confluency before inducing the differentiation. There was no room for the cells in the pristine GelMA to enhance their elongation and reach the cell elongation in the GelMA-PdMGSMWhydrogels. Therefore, we hypothesized that muscle cells in GelMA-PdMGSMW hydrogels would form more myotubes and therefore make more functional muscle tissues compared with those cultured in pristine GelMA hydrogels.

Figure 2f demonstrates the expression levels of genes pertaining to adhesion and proliferation (*i.e.* collagen type I, β1 integrin, and focal adhesion kinase (FAK) genes) and focal adhesion components (*i.e.* vinculin gene) for C2C12 cells cultured in pristine GelMA and GelMA-1.0 mg/mL PdMGSMW hydrogels. A significantly higher expression of underlying genes for the muscle cells cultured in GelMA-1.0 mg/mL PdMGSMW hydrogels was observed compared with that in pristine GelMA hydrogels. For example, β1 integrin gene was expressed 300 times more for the C2C12 myoblasts in GelMA-PdMGSMW gels than that in pristine GelMA gels. These results indicate that GelMA-PdMGSMW hydrogels were more favorable in regulating the adhesion and spreading behaviors of muscle cells compared with pristine GelMA hydrogels most likely because of the biophysical cues of PdMGSMWs in hybrid gels. Enhanced adhesion and spreading of muscle cells in GelMA-PdMGSMW hydrogels compared with pristine GelMA hydrogel are not an electro-active cell specific. Therefore, GelMA-PdMGSMW hydrogels can be used to increase adhesion and spreading of other anchorage-dependent cells.

Pristine GelMA and GelMA-1.0 mg/mL PdMGSMW gels were also evaluated in differentiation of C2C12 myoblasts to myotubes. C2C12 myoblast differentiation cultured in the 3D GelMA gels was confirmed by the immunostaining of α-actin and myosin heavy chain proteins as a standard measure of myotube formation (Figure 3a-3d) [51]. The cross-striation was also observed for both myotubes in pristine GelMA and GelMA-PdMGSMW hydrogels showing maturation of the fabricated muscle tissues (Figure 3a-3d). C2C12 myotubes encapsulated in pristine GelMA and GelMA-1.0 mg/mL PdMGSMW hydrogels were exposed to ES after 8 days of culture for 2 days. Non-stimulated C2C12 myotubes at day 10 of culture were used as the control samples. The contraction movies of electrically stimulated myotubes in both hydrogels were also taken (Supplementary data, Movies S1 and S2). We characterized the contractility of the myotubes using an arbitrary binary number (*i.e.* contraction flag). This number is defined 'one' when the amplitude of myotube contraction exceeds a certain threshold value. Otherwise, it shows 'zero'. The amount of myotube contraction was extracted by analyzing the pixel intensity of the movies captured with a frequency of 5 frames per second. Figure 3e shows the plots of contraction flags versus the frame number for the myotubes grown in pristine GelMA and GelMA-1.0 mg/mL hydrogels. Beating score numbers obtained by the summation of the pulses over time (*i.e.* frame number) were 29 and 68 for the myotubes in the pristine GelMA and the PdMGSMW containing hydrogels, respectively, indicating the myotubes in GelMA-1.0 mg/mL PdMGSMW gels (Supplementary data, Movie S1) had higher contraction compared with those in GelMA gels (Supplementary data, Movie S2). The ES resulted in a continuous contraction of myotubes. Electrophysiological activity and force generation of engineered muscle constructs can be controlled using ES for drug screening and bio-actuator applications [52, 53]. Such engineered tissue models with

controllable differentiation and physiological activity are of potential use for drug discovery applications.

Figure 3f demonstrates the expression of genes related to the maturation and contraction of C2C12 myotubes cultured within pristine GelMA and GelMA containing 1.0 mg/mL PdMGSMWs with/without applying ES. The gene analysis results show that GelMA-1.0 mg/mL PdMGSMW gels enhanced the differentiation and contraction of muscle cells compared with pristine GelMA gels particularly after applying the ES. The effect of electrical conductivity of the gels on the myogenesis process was simply revealed by comparing the maturation of different muscle myotubes (one with applying ES and another without applying ES) cultured in the same gel. Electrical conductivity of hydrogel positively affects the yield of ES for the maturation of muscle myofibers. Accordingly, we concluded that higher maturation of stimulated C2C12 myotubes in the GelMA-PdMGSMW gel compared with that in the pristine GelMA gel is primarily due to higher electrical conductivity of the GelMA-PdMGSMW gel.

SECM is a scanning probe microscopy method that has been used to measure the respiratory activity of biological cells based on redox reactions taking place at the cell-probe interface upon applying a specific potential [54, 55]. Here, SECM was employed to quantify the respiratory activity of C2C12 myotubes cultured in pristine GelMA and GelMA-1.0 mg/mL PdMGSMW hydrogels as shown in Figure 4. The fluxes of oxygen were measured for both non-stimulated and electrically stimulated muscle cells. The measured fluxes were $5.6\pm0.3 \times 10^{-12}$ and $4.4\pm0.5 \times 10^{-12}$ mol cm^{-2} s^{-1} for the C2C12 myotubes in pristine GelMA hydrogels, while these values were $9.5\pm1.3 \times 10^{-12}$ and $1.1\pm0.2 \times 10^{-11}$ mol cm^{-2} s^{-1} for the cells cultured in GelMA-1.0 mg/mL PdMGSMW hydrogels with and without applying the ES, respectively. The latter values are of the order of oxygen fluxes for the embryos [56]. Although the cell density in all cell-laden hydrogels was kept constant at 1×10^7 cells/mL, the possibility of having different cell densities among different hydrogel samples during the oxygen flux measurements could not be ruled out. However, since the Pt microelectrode for the oxygen flux measurements was carefully adjusted on a single myotube, the differences between the oxygen flux values may not be affected by the proliferation rate of muscle cells in the hydrogels. The oxygen flux values were calculated using the Fick's law and the linear relationship of current and distance as shown in Supplementary data, Figure S5. The oxygen mass transfer rate of GelMA and GelMA-1.0 mg/mL PdMGSMW hydrogels as the negative control samples were measured to be $8.3\pm1.9 \times 10^{-13}$ and $7.4\pm2.0 \times 10^{-13}$ mol cm^{-2} s^{-1}, respectively, which are negligible. The results showed that GelMA-PdMGSMW gels significantly improved the metabolic activity of muscle cells compared with pristine GelMA gels. Although some increase was observed in the metabolic activity of cells in the pristine GelMA hydrogel with and without the ES, the metabolic activity of cells in the GelMA-PdMGSMW hydrogel was not affected by the ES. C2C12 metabolism has a direct relationship with cell adhesion [57]. It seems that adding PdMGSMWs to GelMA gels saturated oxygen consumption of cells in the gel. The mesh-like structure of PdMGSMW in the hybrid gels also did not adversely affect nutrient diffusion and thereby metabolic activity of cells in the hybrid gels because the GelMA-PdMGSMW hydrogels always showed a higher respiratory activity in contrast with the pristine GelMA hydrogels. In addition, the oxygen flux measurements for pristine GelMA and GelMA-PdMGSMW hydrogels without cells were not statistically different. In general, SECM can characterize electrochemical behaviors of biological samples with high spatial resolution, locally, and under physiological conditions [56, 58]. Unlike conventional assays to characterize metabolic activity of muscle cells, the SECM provides a rapid and direct measurement of such phenomenon without some uncertainty associated with fluorescence labeling and characterization of muscle cells [59]. Therefore, SECM technique may be used as a powerful and standard measurement to evaluate metabolism of engineered muscle tissues for different applications of muscle tissues *in vitro*, such as drug screening. To this end, diseased muscle tissues can be fabricated and different drug candidates are tested on the tissues. Metabolic response of muscle tissues to different drugs can be recorded and compared using SECM technique as a measure to evaluate the efficiency of each drug for the underlying muscle disease.

Pd is an inert element. However, the presence of Ni and Cu elements in the PdMGSMWs may increase the potential corrosion of the metallic glasses in the culture medium. Here, the leaching of Ni or Cu ions from the PdMGSMWs did not adversely affect the muscle cell function probably due to low concentrations of these ions in the medium. In agreement with our study, Li et al. reported the biocompatibility of $Zr_{61}Ti_2Cu_{25}Al_{12}$ metallic glasses as exposed to L929 fibroblasts, human endothelial cells, and osteoblasts [60]. In another work, Wang et al. showed the biocompatibility of 316 L SS biomedical steel despite its corrosion and leaching of Fe and Ni ions from it [61].

Conclusions

In summary, the PdMGSMWs significantly enhanced the electrical conductivity of pristine GelMA gels. Biocompatible hybrid GelMA-PdMGSMW hydrogels were shown to be more favorable in regulating the adhesion, spreading, and differentiation of encapsulated skeletal muscle cells compared with pristine GelMA gels. Novel GelMA-PdMGSMW hydrogels may find utility in drug screening, development of functional materials for electronics-biology interfaces, and tissue fabrication.

Acknowledgements

This work was supported by the World Premier International Research Center Initiative (WPI), MEXT, Japan.

Supplementary data

Figures S1-S5 and Movies S1 and S2.

References

1 N. Annabi, A. Tamayol, J. A. Uquillas, M. Akbari, L. E. Bertassoni, C. Cha, G. Camci-Unal, M. R. Dokmeci, N. A. Peppas and A. Khademhosseini, *Advanced materials*, 2014, **26**, 85-123.

2 N. A. Peppas, J. Z. Hilt, A. Khademhosseini and R. Langer, *Advanced Materials*, 2006, **18**, 1345-1360.

3 B. V. Slaughter, S. S. Khurshid, O. Z. Fisher, A. Khademhosseini and N. A. Peppas, *Advanced Materials*, 2009, **21**, 3307-3329.

4 D. Mawad, E. Stewart, D. L. Officer, T. Romeo, P. Wagner, K. Wagner and G. G. Wallace, *Advanced Functional Materials*, 2012, **22**, 2692-2699.

5 S. Ahadian, S. Ostrovidov, V. Hosseini, H. Kaji, M. Ramalingam, H. Bae and A. Khademhosseini, *Organogenesis*, 2013, **9**, 87-92.

6 S. Ahadian, J. Ramon-Azcon, H. Chang, X. Liang, H. Kaji, H. Shiku, K. Nakajima, M. Ramalingam, H. Wu, T. Matsue and A. Khademhosseini, *RSC Advances*, 2014, **4**, 9534-9541.

7 S. Ostrovidov, V. Hosseini, S. Ahadian, T. Fujie, S. P. Parthiban, M. Ramalingam, H. Bae, H. Kaji and A. Khademhosseini, *Tissue engineering. Part B, Reviews*, 2014, **20**, 403-436.

8 B. Guo, L. Glavas and A.-C. Albertsson, *Progress in Polymer Science*, 2013, **38**, 1263-1286.

9 X. Yang, L. Qiu, C. Cheng, Y. Wu, Z.-F. Ma and D. Li, *Angewandte Chemie International Edition*, 2011, **50**, 7325-7328.

10 K. T. Sapra and H. Bayley, *Scientific reports*, 2012, **2**, 848.

11 B. Tian, J. Liu, T. Dvir, L. Jin, J. H. Tsui, Q. Qing, Z. Suo, R. Langer, D. S. Kohane and C. M. Lieber, *Nat Mater*, 2012, **11**, 986-994.

12 S. B. Campbell and T. Hoare, *Current Opinion in Chemical Engineering*, 2014, **4**, 1-10.

13 T. Saito, C. C. Wu, H. Shiku, T. Yasukawa, M. Yokoo, T. Ito-Sasaki, H. Abe, H. Hoshi and T. Matsue, *The Analyst*, 2006, **131**, 1006-1011.

14 J. S. Im, B. Bai and Y. S. Lee, *Biomaterials*, 2010, **31**, 1414-1419.

15 A. Servant, C. Bussy, K. Al-Jamal and K. Kostarelos, *Journal of Materials Chemistry B*, 2013, **1**, 4593-4600.

16 S. R. Shin, H. Bae, J. M. Cha, J. Y. Mun, Y.-C. Chen, H. Tekin, H. Shin, S. Farshchi, M. R. Dokmeci, S. Tang and A. Khademhosseini, *ACS Nano*, 2012, **6**, 362-372.

17 J. Ramon-Azcon, S. Ahadian, M. Estili, X. Liang, S. Ostrovidov, H. Kaji, H. Shiku, M. Ramalingam, K. Nakajima, Y. Sakka, A. Khademhosseini and T. Matsue, *Advanced materials*, 2013, **25**, 4028-4034.

18 J.-O. You, M. Rafat, G. J. C. Ye and D. T. Auguste, *Nano Letters*, 2011, **11**, 3643-3648.

19 A. M. Martins, G. Eng, S. G. Caridade, J. F. Mano, R. L. Reis and G. Vunjak-Novakovic, *Biomacromolecules*, 2014, **15**, 635-643.

20 S. R. Shin, B. Aghaei-Ghareh-Bolagh, T. T. Dang, S. N. Topkaya, X. Gao, S. Y. Yang, S. M. Jung, J. H. Oh, M. R. Dokmeci, X. S. Tang and A. Khademhosseini, *Advanced materials*, 2013, **25**, 6385-6391.

21 T. Fujie, S. Ahadian, H. Liu, H. Chang, S. Ostrovidov, H. Wu, H. Bae, K. Nakajima, H. Kaji and A. Khademhosseini, *Nano Letters*, 2013, **13**, 3185-3192.

22 M. Chen, *NPG Asia Materials*, 2011, **3**, 82-90.

23 M. Telford, *Materials Today*, 2004, **7**, 36-43.

24 L. Huang, D. Qiao, B. A. Green, P. K. Liaw, J. Wang, S. Pang and T. Zhang, *Intermetallics*, 2009, **17**, 195-199.

25 M. L. Morrison, R. A. Buchanan, R. V. Leon, C. T. Liu, B. A. Green, P. K. Liaw and J. A. Horton, *Journal of biomedical materials research. Part A*, 2005, **74**, 430-438.

26 K. S. Nakayama, Y. Yokoyama, T. Ono, M. W. Chen, K. Akiyama, T. Sakurai and A. Inoue, *Advanced Materials*, 2010, **22**, 872-875.

27 K. S. Nakayama, Y. Yokoyama, T. Wada, N. Chen and A. Inoue, *Nano Letters*, 2012, **12**, 2404-2407.

28 K. S. Nakayama, Y. Yokoyama, G. Xie, Q. S. Zhang, M. W. Chen, T. Sakurai and A. Inoue, *Nano Letters*, 2008, **8**, 516-519.

29 S. Kajita, S.-I Yamaura, H. Kimura, K. Yubuta, A. Inoue, *IEEJ Transac. Sensors Micromachines* 2008, **28**, 225-229.

30 J. Ramon-Azcon, S. Ahadian, R. Obregon, G. Camci-Unal, S. Ostrovidov, V. Hosseini, H. Kaji, K. Ino, H. Shiku, A. Khademhosseini and T. Matsue, *Lab on a chip*, 2012, **12**, 2959-2969.

31 O. Haruyama, T. Watanabe, K. Yuki, M. Horiuchi, H. Kato and N. Nishiyama, *Physical Review B*, 2011, **83**, 064201.

32 D. Wang, S. Fujinami, H. Liu, K. Nakajima and T. Nishi, *Macromolecules*, 2010, **43**, 9049-9055.

33 J. L. Hutter and J. Bechhoefer, *Review of Scientific Instruments*, 1993, **64**, 1868-1873.

34 B. V. Derjaguin, V. M. Muller and Y. P. Toporov, *Journal of Colloid and Interface Science*, 1975, **53**, 314-326.

35 S. Ahadian, J. Ramon-Azcon, S. Ostrovidov, G. Camci-Unal, H. Kaji, K. Ino, H. Shiku, A. Khademhosseini and T. Matsue, *Biomedical microdevices*, 2013, **15**, 109-115.

36 R. Obregon, S. Ahadian, J. Ramon-Azcon, L. Chen, T. Fujita, H. Shiku, M. Chen and T. Matsue, *Biosensors & bioelectronics*, 2013, **50**, 194-201.

37 S. Ahadian, J. Ramon-Azcon, S. Ostrovidov, G. Camci-Unal, V. Hosseini, H. Kaji, K. Ino, H. Shiku, A. Khademhosseini and T. Matsue, *Lab on a chip*, 2012, **12**, 3491-3503.

38 C. Handschin, A. Mortezavi, J. Plock and D. Eberli, *Advanced drug delivery reviews*, 2015, **82-83**, 168-175.

39 S. R. Ryoo, Y. K. Kim, M. H. Kim and D. H. Min, *ACS Nano*, 2010, **4**, 6587-6598.

40 T. D. Schmittgen and K. J. Livak, *Nature protocols*, 2008, **3**, 1101-1108.

41 Y. Matsumae, Y. Takahashi, K. Ino, H. Shiku and T. Matsue, *Analytica Chimica Acta*, 2014, **842**, 20-26.

42 Y. S. Torisawa, Y. Nashimoto, T. Yasukawa, H. Shiku and T. Matsue, *Biotechnology and bioengineering*, 2007, **97**, 615-621.

43 N. Tandon, A. Marsano, R. Maidhof, K. Numata, C. Montouri-Sorrentino, C. Cannizzaro, J. Voldman and G. Vunjak-Novakovic, *Lab on a chip*, 2010, **10**, 692-700.

44 H. Aubin, J. W. Nichol, C. B. Hutson, H. Bae, A. L. Sieminski, D. M. Cropek, P. Akhyari and A. Khademhosseini, *Biomaterials*, 2010, **31**, 6941-6951.

45 L. Huang, Z. Cao, H. M. Meyer, P. K. Liaw, E. Garlea, J. R. Dunlap, T. Zhang and W. He, *Acta Biomater.*, 2011, **7**, 395-405.

46 N. Kaushik, P. Sharma, S. Ahadian, A. Khademhosseini, M. Takahashi, A. Makino, S. Tanaka and M. Esashi, *Journal of Biomedical Materials Research Part B: Applied Biomaterials*, 2014, DOI: 10.1002/jbm.b.33135, n/a-n/a.

47 N. T. Kirkland, N. Birbilis and M. P. Staiger, *Acta Biomater.*, 2012, **8**, 925-936.

48 B. Zberg, P. J. Uggowitzer and J. F. Loffler, *Nat. Mater.*, 2009, **8**, 887-891.

49 H. Musa, C. Orton, E. E. Morrison and M. Peckham, *J. Muscle Res. Cell Motil.*, 2003, **24**, 303-310.

50 N. T. Swailes, M. Colegrave, P. J. Knight and M. Peckham, *J. Cell Sci.*, 2006, **119**, 3561-3570.
51 S. Ahadian, J. Ramón-Azcón, M. Estili, X. Liang, S. Ostrovidov, H. Shiku, M. Ramalingam, K. Nakajima, Y. Sakka, H. Bae, T. Matsue and A. Khademhosseini, *Sci. Rep.*, 2014, **4**.
52 S. Ahadian, J. Ramón-Azcón, M. Estili, R. Obregón, H. Shiku and T. Matsue, *Biosens. Bioelectron.*, 2014, **59**, 166-173.
53 J. C. Nawroth, H. Lee, A. W. Feinberg, C. M. Ripplinger, M. L. McCain, A. Grosberg, J. O. Dabiri and K. K. Parker, *Nat Biotech*, 2012, **30**, 792-797.
54 Y. Matsumae, T. Arai, Y. Takahashi, K. Ino, H. Shiku and T. Matsue, *Chem. Commun.*, 2013, **49**, 6498-6500.
55 Y. Takii, K. Takoh, M. Nishizawa and T. Matsue, *Electrochim. Acta*, 2003, **48**, 3381-3385.
56 H. Shiku, T. Shiraishi, S. Aoyagi, Y. Utsumi, M. Matsudaira, H. Abe, H. Hoshi, S. Kasai, H. Ohya and T. Matsue, *Anal. Chim. Acta*, 2004, **522**, 51-58.
57 E. Smith, J. Yang, L. McGann, W. Sebald and H. Uludag, *Biomaterials*, 2005, **26**, 7329-7338.
58 H. Shiku, T. Arai, Y. Zhou, N. Aoki, T. Nishijo, Y. Horiguchi, K. Ino and T. Matsue, *Mol. BioSyst.*, 2013, **9**, 2701-2711.
59 M. T. Wolf, K. A. Daly, J. E. Reing and S. F. Badylak, *Biomaterials*, 2012, **33**, 2916-2925.
60 J. Li, L.-l. Shi, Z.-d. Zhu, Q. He, H.-j. Ai and J. Xu, Materials Science and Engineering: C, 2013, 33, 2113-2121.
61 Y. B. Wang, H. F. Li, Y. F. Zheng and M. Li, Materials Science and Engineering: C, 2012, 32, 599-606.

Figure captions

Figure 1. Morphology of PdMGSMWs and electrical and mechanical characteristics of GelMA and GelMA-PdMGSMW hydrogels. **(a)** SEM micrographs of fabricated PdMGSMWs. **(b)** Histogram of size distribution of the PdMGSMWs. **(c-1)** I-V curves of hydrogels obtained by performing a DC double voltage sweep. **(c-2)** Magnitude and phase Bode plots of the impedance spectra obtained from devices containing pristine GelMA, GelMA-0.5 mg/mL PdMGSMW, and GelMA-1.0 mg/mL PdMGSMW hydrogels. **(c-3)** Parallel capacitance and resistance as a function of frequency for underlying hydrogels extracted from the impedance data together with schematic of a Randels' equivalent circuit representing hydrogels. **(d)** Young's moduli of pristine and hybrid GelMA versus the concentration of PdMGSMWs. Asterisk indicates a significant difference between samples (*$p < 0.05$).

Figure 2. Fluorescence and phase images obtained from immunostained fibroblasts and C2C12 myoblasts to evaluate cell viability and elongation and gene expression of C2C12 myoblasts embedded in pristine GelMA and hybrid GelMA-1.0 mg/mL PdMGSMW hydrogels. **(a)** Fibroblasts cultured within pristine GelMA and GelMA-1.0 mg/mL PdMGSMW hydrogels at days 1 and 2 of culture. **(b)** C2C12 myoblasts in pristine GelMA gel and evidence of elongation of C2C12 myoblasts attached to PdMGSMWs in hybrid GelMA-PdMGSMW hydrogels. Insets in the two right panels show a magnified phase image of the framed area. **(c)** Viability of fibroblasts encapsulated in pristine GelMA and GelMA-1.0 mg/mL PdMGSMW hydrogels at two consecutive days of culture. **(d)** Number of viable C2C12 myoblasts relative to day 1 in pristine GelMA and GelMA-1.0 mg/mL PdMGSMW hydrogels. **(e)** Aspect ratios of C2C12 myoblasts in pristine GelMA and GelMA-1.0 mg/mL PdMGSMW hydrogels at 2 different days of culture. **(f)** The expression levels of genes pertaining to adhesion, proliferation, and focal adhesion components as normalized to that of GAPDH gene. Asterisks indicate significant differences between samples (*$p < 0.05$).

Figure 3. Immunostaining of C2C12 myotubes and gene expression analysis data. Fluorescent images of immunostained myotubes (without applying the ES) in pristine GelMA and hybrid GelMA-1.0 mg/mL PdMGSMW hydrogels to reveal cell nuclei/F-actin **(a, c)** and cell nuclei/myosin heavy chain **(b, d)**. Striated myotubes are shown in the bottom of panels. **(e)** Movie analysis of contractile myotubes cultured in pristine GelMA and hybrid GelMA-1.0 mg/mL PdMGSMW hydrogels. **(f)** Gene expression of myotubes embedded in pristine GelMA and hybrid GelMA-1.0 mg/mL PdMGSMW hydrogels. The expression levels of genes were normalized to that of GAPDH gene. The ES parameters were voltage 4 V, frequency 1 Hz, and duration 10 ms applied at day 8 of culture for 2 continuous days. Asterisks indicate significant differences between samples (*$p < 0.05$).

Figure 4. Oxygen flux measurement of pristine GelMA and hybrid GelMA-1.0 mg/mL PdMGSMW hydrogels and C2C12 myotubes in pristine GelMA and hybrid GelMA-1.0 mg/mL PdMGSMW hydrogels. **(a)** Schematic representation of the SECM setup to measure the oxygen flux of underlying samples. **(b)** Oxygen flux values of pristine GelMA and hybrid GelMA-1.0 mg/mL PdMGSMW hydrogels and C2C12 myotubes in pristine GelMA and GelMA-1.0 mg/mL PdMGSMW hydrogels with and without applying the electrical stimulation denoted as +ES and -ES, respectively. Asterisks indicate significant differences between samples (*$p < 0.05$).

Table 1. Resistivities of the hybrid hydrogels versus the concentration of PdMGSMWs.

PdMGSMWconcentration (mg/mL)	Resistivity at 100 Hz (Ω·cm)
0	1050
0.5	69.80
1.0	40.00

Table 2. Primer sequences

β1 integrin	5′-GACCTGCCTTGGTGTCTGTGC-3′	5′-AGCAACCACACCAGCTACAAT-3′
vinculin	5′-AGCAGGAGTTGACTCACCAG-3′	5′-TCTAAGATCTGCCTGATGGC-3′
collagen type I	5′-ACTGGTACATCAGCCCGAAC-3′	5′-GGTGGAGGGAGTTTACACGA-3′
FAK	5′-GTAGTGAGCCAACCACCTGG-3′	5′-GCCCTTGTCTGTCAGGTAAC-3′
MRF4	5′-CGAAAGGAGGAGACTAAAG-3′	5′-CTGTAGACGCTCAATGTAG-3′
myogenin	5′-TGTCTGTCAGGCTGGGTGTG-3′	5′-TCGCTGGGCTGGGTGTTAG-3′
α-actinin	5′-TCATCCTCCGCTTCGCCATTC-3′	5′-CTTCAGCATCCAACATCTTAGG-3′
sarcomeric actin	5′-ATGGTAGGTATGGGTCAG-3′	5′-GATCTTCTCCATGTCGTC-3′
MHCIId/x	5′-GCGACAGACACCTCCTTCAAG-3′	5′-TCCAGCCAGCCAGCGATG-3′

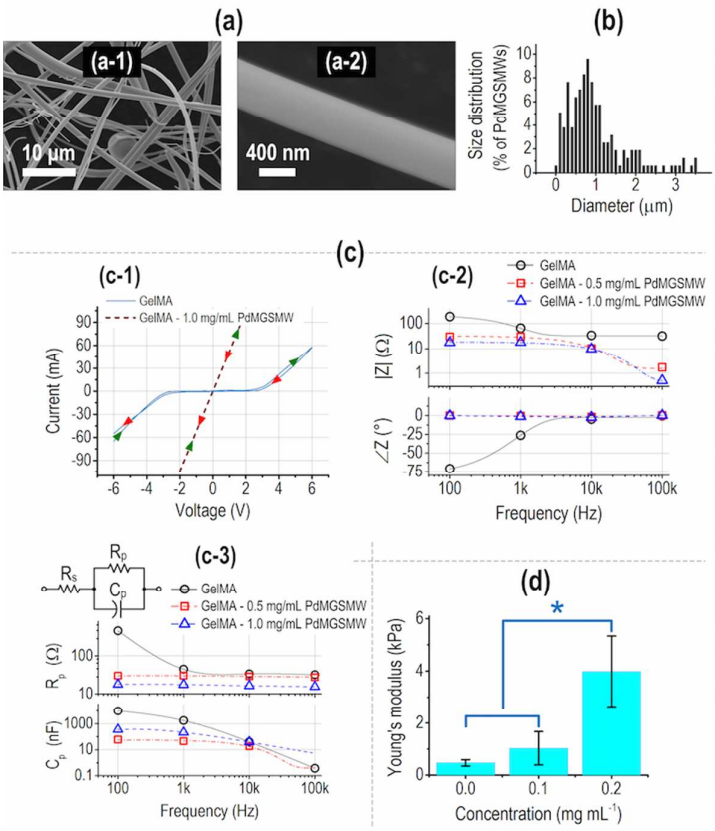

Figure 1

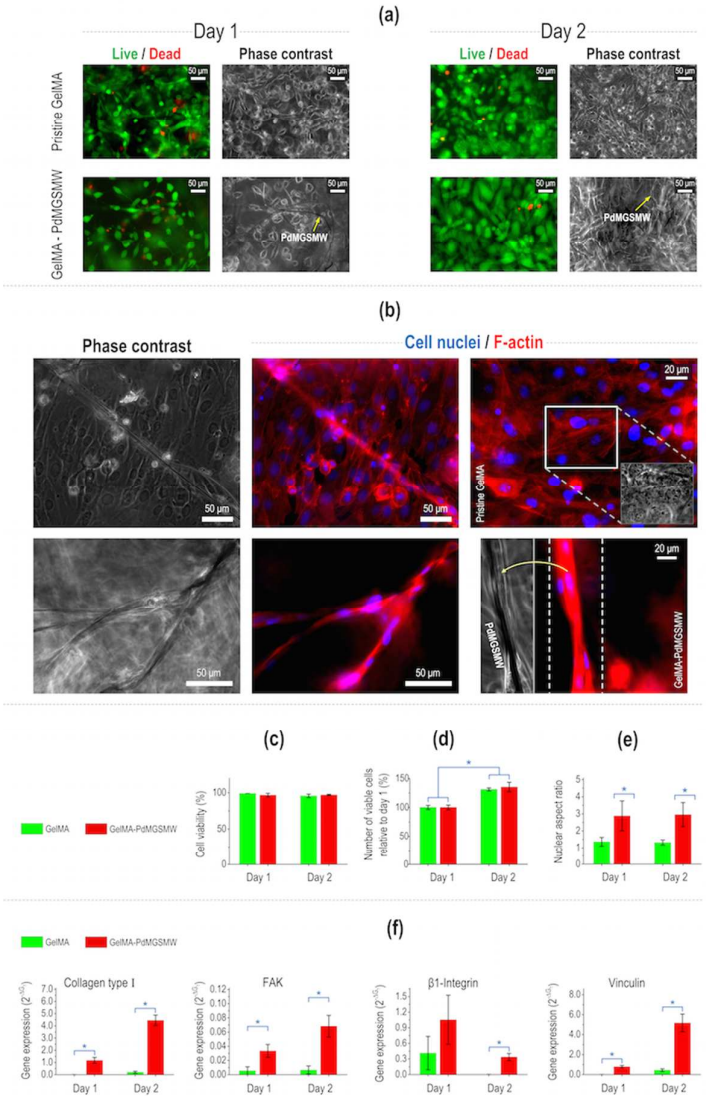
(a)
Day 1
Day 2
Live / Dead
Phase contrast
Pristine GelMA
GelMA - PdMGSMW
PdMGSMW
(b)
Phase contrast
Cell nuclei / F-actin
(c)
(d)
(e)
GelMA
GelMA-PdMGSMW
Cell viability (%)
Number of viable cells relative to day 1 (%)
Nuclear aspect ratio
Day 1
Day 2
(f)
Collagen type I
FAK
β1-Integrin
Vinculin
Gene expression

Figure 2

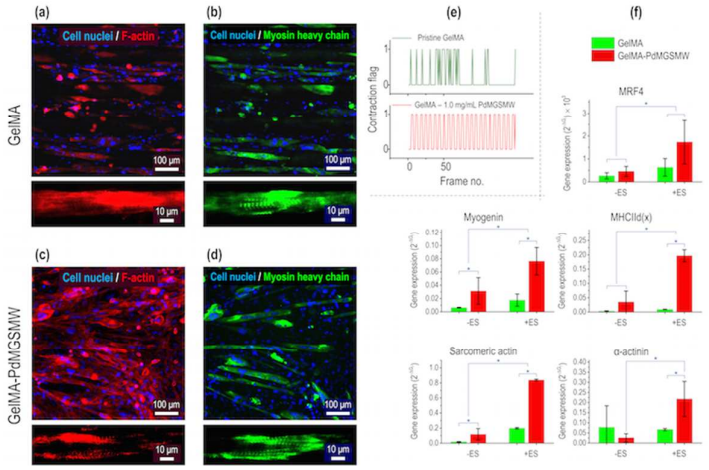

Figure 3

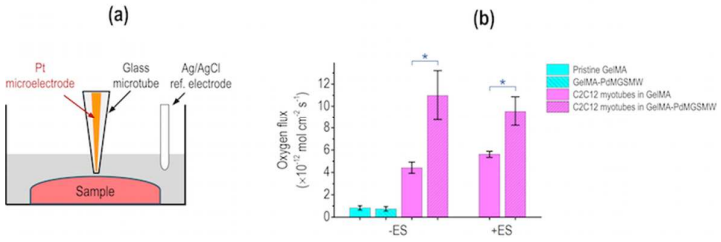
(a)
Pt microelectrode
Glass microtube
Ag/AgCl ref. electrode
Sample
(b)
Oxygen flux (×10⁻¹² mol cm⁻² s⁻¹)
0
2
4
6
8
10
12
-ES
+ES
*
*
Pristine GelMA
GelMA-PdMGSMW
C2C12 myotubes in GelMA
C2C12 myotubes in GelMA-PdMGSMW

Figure 4

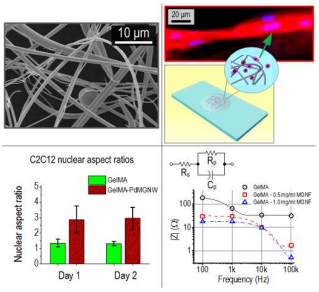

Hybrid Pd-based metallic glass sub-micron wires-hydrogel scaffolds are efficient in regulating behaviors of skeletal muscle cells.